

Exploring the top and bottom of the quantum control landscape

Vincent Beltrani,^{a)} Jason Dominy,^{b)} Tak-San Ho,^{a)} and Herschel Rabitz^{a)}

^{a)} Department of Chemistry, Princeton University, Princeton NJ 08544

^{b)} Program in Applied and Computational Mathematics, Princeton University, Princeton NJ

08544

(Received

Abstract

A controlled quantum system possesses a search landscape defined by the target physical objective as a function of the controls. This paper focuses on the landscape for the transition probability $P_{i \rightarrow f}$ between the states of a finite level quantum system. Traditionally, the controls are applied fields; here we extend the notion of control to also include the Hamiltonian structure, in the form of time independent matrix elements. Level sets of controls that produce the same transition probability value are shown to exist at the bottom $P_{i \rightarrow f} = 0.0$ and top $P_{i \rightarrow f} = 1.0$ of the landscape with the field and/or Hamiltonian structure as controls. We present an algorithm to continuously explore these level sets starting from an initial point residing at either extreme value of $P_{i \rightarrow f}$. The technique can also identify control solutions that exhibit the desirable properties of (a) robustness at the top and (b) the ability to rapidly rise towards an optimal control from the bottom. Numerical simulations are presented to illustrate the varied control behavior at the top and bottom of the landscape for several simple model systems.

1 Introduction

Control of quantum phenomena is garnering increasing attention as growing numbers of experimental studies indicate the ability to find effective control over a broad range of quantum systems [1]. Successful experiments using shaped laser pulses include selective bond breaking [2], selective excitation of extremely similar species [3], control of optical switches in semiconductors [4], selective energy transfer in bio-molecules [5], the manipulation of electron excitation [6], etc.

The control landscape is defined as the physical observable as a function of the control variables. The general structure of the landscape dictates the ease of finding good controls as well as robustness to noise and other characteristics of a controlled quantum system. Thus, exploration of the landscape is important, and the tools developed in this work are applicable to general quantum observables. For illustration, this paper considers the transition probability, $P_{i \rightarrow f}$, from state $|i\rangle$ to $|f\rangle$. The transition probability landscape has been shown [7, 8, 9, 10, 11] to generally exhibit a fundamental trap-free topology for completely controllable quantum systems, i.e., satisfaction of certain physical assumptions assures that there are no sub-optimal extrema capable of halting gradient based optimizations [12, 13, 14]. Large, even infinite, numbers of control solutions are capable of achieving the same observable value defining members of a quantum control level set. Traditionally, the controls have taken the form of electromagnetic fields applied to a fixed physical system. In contrast, a recent study treated the Hamiltonian structure (i.e., time independent matrix elements) as the controls [11]. In this circumstance, the Hamiltonian structure in the laboratory can be varied, for example, by substituting one functional group for another bonded to a molecular scaffold or by altering the relative composition of a material sample. Figure 1 shows the selection options for control variables. Depending on the control scenario, the applied field (Fig. 1a) or the Hamiltonian structure (Fig. 1b) may be viewed as the control. The most general scenario (Fig. 1c) considers both the Hamiltonian structure and the

applied field as dual controls. Exploiting this rich flexibility could be important in order to meet particularly demanding objectives (e.g., prescribed complex responses from a non-linear optical material).

Control level sets, over the interior domain $0 < P_{i \rightarrow f} < 1$, have been investigated through a first-order (i.e., through the use of the gradient of $P_{i \rightarrow f}$ with respect to the controls) numerical algorithm called D-MORPH [9, 10, 15]. The solution to the D-MORPH differential equation permits exploration of the connected members of the control level sets. The landscape top $P_{i \rightarrow f} = 1.0$ and bottom $P_{i \rightarrow f} = 0.0$ have particular physical relevance. The top is the most desired location while at the bottom the goal is to climb away as rapidly as possible. In order to explore level sets at the top or bottom, this work generalizes the original first-order D-MORPH algorithm to produce a new second-order formulation. This extended D-MORPH algorithm utilizes the Hessian as the second derivative of $P_{i \rightarrow f}$ with respect to the control variables. At both landscape extremes, the Hessian has a large number of zero eigenvalues and associated eigenvectors that span the Hessian null space. The eigenvectors spanning the null space describe local coordinated variations of the controls that leave the $P_{i \rightarrow f}$ value fixed. The second-order D-MORPH algorithm systematically makes such changes of the controls in these null spaces to continuously explore the level sets at the landscape top or bottom. At this early stage of landscape feature exploration, the myopic nature of D-MORPH based simulations are important to link with the associated theoretical analyses and provide a foundation for subsequent laboratory landscape excursions with a variety of possible algorithms.

The remainder of the paper is organized as follows: Section 2 presents the general formulation of the gradient and Hessian of the transition probability with respect to the controls. Utilizing the gradient and Hessian, Section 3 summarizes the algorithm used to explore the top and bottom of the $P_{i \rightarrow f}$ landscape. Section 4 presents numerical results using simple few level systems for illustration, and Section 5 offers concluding remarks on the significance of the work.

2 Transition Probability Landscape

Throughout the paper, the symbol β will be used to indicate collectively the set of all the control parameters in the system $\beta_j, j = 1, 2, \dots, M$, i.e., $\beta \in \mathbb{R}^M$. These M control parameters may be drawn from any component of the Hamiltonian under consideration. For example, these parameters may consist of the field spectral amplitudes and phases, as well as the Hamiltonian structure itself, i.e., the dipole matrix elements and system energy levels. The collective controls, β , can be considered within the same unified framework regardless of their specific nature in the Hamiltonian which will be written as $H(\beta, t)$. In the remainder of the paper, a control that produces an interior yield $0 < P_{i \rightarrow f} < 1$ will be denoted as β , while a control producing either $P_{i \rightarrow f} = 0.0$ or $P_{i \rightarrow f} = 1.0$ will be written as β^* .

The transition probability landscape is defined by $P_{i \rightarrow f}(\beta)$ as a function of β

$$P_{i \rightarrow f}(\beta) = |\langle f | U(T, 0) | i \rangle|^2. \quad (1)$$

Here, $U(T, 0)$ is the propagator evaluated at the target time T , governed by the Schrödinger equation

$$i\hbar \frac{\partial}{\partial t} U(t, 0) = H(\beta, t) U(t, 0), \quad U(0, 0) = 1. \quad (2)$$

The propagator $U(t, 0)$ is implicitly dependent on β through the Hamiltonian $H(\beta, t)$ in Eq. 2. The system has N states and we assume that the initial and target states, $|i\rangle$ and $|f\rangle$, respectively, are orthogonal, $\langle f | i \rangle = 0$.

Below, we construct the first and second derivatives of the propagator $U(t, 0)$ with respect to the parameters β , as they are needed for the remainder of the landscape analysis. On differentiating Eq. 2 with respect to an arbitrary parameter β_j , we obtain

$$i\hbar \frac{\partial}{\partial t} U_{\beta_j}(t, 0) = H_{\beta_j}(\beta, t) U(t, 0) + H(\beta, t) U_{\beta_j}(t, 0), \quad (3)$$

with initial conditions $U_{\beta_j}(0, 0) = 0$, where we use the notation $U_{\beta_j}(t, 0) \equiv \partial U(t, 0)/\partial \beta_j$ and $H_{\beta_j}(\beta, t) \equiv \partial H(\beta, t)/\partial \beta_j$. Equation 3 is an inhomogeneous equation with a homogeneous part identical to Eq. 2. Thus, the solution to Eq. 3 can be written as [16, 17]

$$U_{\beta_j}(t, 0) = (-i/\hbar)U(t, 0) \int_0^t dt' U^\dagger(t', 0)H_{\beta_j}(\beta, t')U(t', 0). \quad (4)$$

The second order derivatives $U_{\beta_i\beta_j}(t, 0) \equiv \partial^2 U(t, 0)/\partial \beta_i\partial \beta_j$ can be derived similarly by differentiating Eq. 3 and utilizing Eqs. 2 and 4. Here, we only present the result:

$$\begin{aligned} U_{\beta_i\beta_j}(t, 0) = & (-i/\hbar)U(t, 0) \int_0^t dt' U^\dagger(t', 0)[H_{\beta_i\beta_j}(\beta, t')U(t', 0) \\ & + H_{\beta_i}(\beta, t')U_{\beta_j}(t', 0) + H_{\beta_j}(\beta, t')U_{\beta_i}(t', 0)], \end{aligned} \quad (5)$$

where $H_{\beta_i\beta_j}(\beta, t) \equiv \partial^2 H(\beta, t)/\partial \beta_i\partial \beta_j$.

2.1 Gradient of the Transition Probability Landscape

We consider here a control β corresponding to a point on the landscape where $P_{i \rightarrow f}(\beta)$ is not 0.0 or 1.0. The behavior of the landscape in the neighborhood of such a control β can be explored by expanding $P_{i \rightarrow f}(\beta + d\beta)$ to first order

$$P_{i \rightarrow f}(\beta + d\beta) \approx P_{i \rightarrow f}(\beta) + \sum_{j=1}^M \frac{\partial P_{i \rightarrow f}(\beta)}{\partial \beta_j} d\beta_j \quad (6a)$$

$$= P_{i \rightarrow f}(\beta) + \nabla P_{i \rightarrow f}(\beta)^\top \cdot d\beta \quad (6b)$$

where the first derivative of the transition probability, $\partial P_{i \rightarrow f}(\beta)/\partial \beta_j$, is given by

$$\begin{aligned} \partial P_{i \rightarrow f}(\beta)/\partial \beta_j = & \frac{\partial}{\partial \beta_j} |\langle f|U(T, 0)|i\rangle|^2 \\ = & \langle i|U_{\beta_j}^\dagger(T, 0)|f\rangle \langle f|U(T, 0)|i\rangle + \langle i|U^\dagger(T, 0)|f\rangle \langle i|U_{\beta_j}(T, 0)|i\rangle \end{aligned} \quad (7)$$

$$= (2/\hbar) \int_0^T \text{Im}[\langle \chi|U^\dagger(t, 0)H_{\beta_j}(\beta, t)U(t, 0)|i\rangle] dt. \quad (8)$$

In Eq. 6b, ‘ \top ’ denotes the vector transpose operation and the gradient $\nabla P_{i \rightarrow f}(\beta)$ will be used as a compact notation throughout the paper. Equation 4 was used on going from Eq. 7 to Eq. 8 where $|\chi\rangle \equiv U^\dagger(T, 0)|f\rangle\langle f|U(T, 0)|i\rangle$. The first order derivative in Eq. 8 is useful for guiding the control β to either extremum $P_{i \rightarrow f} = 0.0$ or $P_{i \rightarrow f} = 1.0$.

2.2 Hessian of the Transition Probability Landscape

The top or bottom of the landscape is an extremum with a corresponding control β^* satisfying $\partial P_{i \rightarrow f}(\beta^*)/\partial \beta_j^* = 0$ for $j = 1, \dots, M$. The behavior in the neighborhood of an extremum can be explored by expanding $P_{i \rightarrow f}(\beta^* + d\beta)$ to second order

$$P_{i \rightarrow f}(\beta^* + d\beta) \approx P_{i \rightarrow f}(\beta^*) + \frac{1}{2} \sum_{j=1}^M \sum_{k=1}^M d\beta_j \frac{\partial^2 P_{i \rightarrow f}(\beta^*)}{\partial \beta_j^* \partial \beta_k^*} d\beta_k, \quad (9)$$

where the second derivatives of the transition probability, $\partial^2 P_{i \rightarrow f}(\beta)/\partial \beta_i \partial \beta_j$, may be calculated by differentiating Eq. 8 with respect to β_k , leading to the general expression

$$\begin{aligned} \partial^2 P_{i \rightarrow f}(\beta)/\partial \beta_i \partial \beta_j &= 2\text{Re}\{\langle i|U^\dagger(T, 0)|f\rangle\langle f|U_{\beta_i \beta_j}(T, 0)|i\rangle \\ &+ \langle i|U_{\beta_i}^\dagger(T, 0)|f\rangle\langle f|U_{\beta_j}(T, 0)|i\rangle\}. \end{aligned} \quad (10)$$

Equation 10 applies at any point on the landscape and Sections 2.2.1 and 2.2.3 will, respectively, specialize this result to cases at the top and bottom. We can conveniently write Eq. 9 in matrix-vector form as

$$P_{i \rightarrow f}(\beta^* + d\beta) \approx P_{i \rightarrow f}(\beta^*) + (1/2) d\beta^\top \cdot \nabla^2 P_{i \rightarrow f}(\beta^*) \cdot d\beta. \quad (11)$$

In Eq. 11, $\nabla^2 P_{i \rightarrow f}(\beta^*) \in \mathbb{R}^{M \times M}$ is the Hessian matrix, i.e., the matrix of second partial derivatives with respect to the system parameters, evaluated at β^* .

2.2.1 Hessian at the Top of the Landscape

Previous formal work [17, 18] showed that multiple control solutions can exist at the top of the landscape where $P_{i \rightarrow f} = 1.0$. The Hessian at the top can facilitate exploration of the family of control solutions there. In particular, at the top of the landscape, $U(T)|i\rangle = e^{i\theta}|f\rangle$ for some phase $\theta \in [0, 2\pi)$, and substituting this relationship into Eq. 10 upon using Eqs. 4 and 5 leads to the result

$$\begin{aligned} \frac{\partial^2 P_{i \rightarrow f}}{\partial \beta_j^* \partial \beta_k^*} &= (-2/\hbar^2) \sum_{p \neq i} \text{Re} \left[\int_0^T \langle p | U^\dagger(t, 0) H_{\beta_j^*}(\beta^*, t) U(t, 0) | i \rangle dt \right. \\ &\quad \left. \times \int_0^T \langle i | U^\dagger(t, 0) H_{\beta_k^*}(\beta^*, t) U(t, 0) | p \rangle dt \right]. \end{aligned} \quad (12)$$

In order to reveal the structure of the Hessian, we define the set of $2N - 2$ vectors: $v_p(\beta^*), w_p(\beta^*)$ for $p = 1, \dots, i-1, i+1, \dots, N$. Each of the vectors is of length M with the j -th component being

$$[v_p(\beta^*)]_j = \frac{\sqrt{2}}{\hbar} \int_0^T \text{Re}[\langle p | U^\dagger(t, 0) H_{\beta_j^*}(\beta^*, t) U(t, 0) | i \rangle] dt \quad (13a)$$

$$[w_p(\beta^*)]_j = \frac{\sqrt{2}}{\hbar} \int_0^T \text{Im}[\langle p | U^\dagger(t, 0) H_{\beta_j^*}(\beta^*, t) U(t, 0) | i \rangle] dt. \quad (13b)$$

The Hessian matrix with elements in Eq. 12 may now be written explicitly in terms of these vectors as

$$\nabla^2 P_{i \rightarrow f}(\beta^*) = - \sum_{p \neq i} [v_p(\beta^*) \cdot v_p^\top(\beta^*) + w_p(\beta^*) \cdot w_p^\top(\beta^*)]. \quad (14)$$

Equation 14 shows that the Hessian is a sum of $2N - 2$ rank one matrices. If the set $\{v_p(\beta^*), w_p(\beta^*)\}_{p \neq i}$ is linearly independent, then the Hessian will have rank $2N - 2$; otherwise the rank is less than $2N - 2$. This result has important practical consequences for optimal control, as shown in the following subsections.

2.2.2 Robustness at the Top of the Landscape

A physically attractive control β^* is one that consistently produces high yields even in the presence of some degree of noise around β^* at or near the top of the landscape. In the general context considered here noise may correspond to statistical variation in the field and/or uncertainty in the time independent Hamiltonian structure. Below, we show that the trace of the Hessian may be utilized as a scalar measure of the deviation of $P_{i \rightarrow f}$ around a control β^* .

In order to analyze the behavior at the top of the landscape, consider an arbitrary variation $d\beta$ about β^* expressed as

$$d\beta = \sum_{j=1}^M db_j u_j(\beta^*) \quad (15)$$

where $\{db_j\}_{j=1,\dots,M}$ are real expansion coefficients and the set of $u_j(\beta^*)$ for $j = 1, \dots, M$ are the eigenvectors of $\nabla^2 P_{i \rightarrow f}(\beta^*)$ satisfying

$$\nabla^2 P_{i \rightarrow f}(\beta^*) \cdot u_j(\beta^*) = \sigma_j u_j(\beta^*), \quad j = 1, \dots, M. \quad (16)$$

Importantly, only the first $2N - 2$ of the eigenvalues σ_j are non-zero [11, 17, 18]. Here we assume the likely circumstance that $M \geq 2N - 2$; violation of the latter criteria will limit free variations on the landscape possibly leading to *false* traps on the otherwise nominally trap-free landscape. Practical circumstances will likely entail $M \approx N^2$ easily satisfying $M \geq 2N - 2$. Equation 15 utilizes the fact that the eigenvectors of the Hessian form a complete set in the M -dimensional space of controls and the expansion coefficients in Eq. 15 may be interpreted as the projection of the control noise along each eigen-direction of the Hessian. The norm squared of $d\beta$ is given by

$$\|d\beta\|^2 \equiv (d\beta)^\top d\beta = \sum_{j=1}^M (db_j)^2. \quad (17)$$

The effect of a control variation $d\beta$ in Eq. 15 is given by Eq. 11

$$\Delta P_{i \rightarrow f}(\beta^*) = (1/2) \sum_{j=1}^M \sigma_j (db_j)^2 \quad (18)$$

$$= (1/2) \sum_{j=1}^{2N-2} \sigma_j (db_j)^2 \quad (19)$$

where we have utilized the fact that only the first $2N - 2$ eigenvalues of the Hessian are non-zero [17, 18]. In order to appreciate the significance of Eq. 19, we make the physically reasonable assumption that the noise is equally distributed along each eigen-direction of the Hessian such that $(db_j)^2 = (db_k)^2$ for all $j, k = 1, \dots, M$. Defining $\|d\beta\|^2 = (d\beta_0)^2$, then it follows from Eq. 17 that $db_j = \pm[(d\beta_0)^2/M]^{1/2}$ and Eq. 19 becomes

$$\Delta P_{i \rightarrow f}(\beta^*) = \left(\frac{(d\beta_0)^2}{2M} \right) \text{Tr}[\nabla^2 P_{i \rightarrow f}(\beta^*)], \quad (20)$$

since the trace of a matrix is equivalent to the sum of its eigenvalues. Utilizing Eq. 14 the deviation in Eq. 20 can be re-written

$$\Delta P_{i \rightarrow f}(\beta^*) = - \left(\frac{(d\beta_0)^2}{M\hbar^2} \right) \sum_{p \neq i} \sum_{j=1}^M \left| \int_0^T \langle p | U^\dagger(t, 0) H_{\beta_j^*}(\beta^*, t) U(t, 0) | i \rangle dt \right|^2. \quad (21)$$

Equations 20 or 21 show the relationship between the transition probability deviation, $\Delta P_{i \rightarrow f}(\beta^*)$, at the top of the landscape and the Hessian trace there. In the worst case scenario, the disturbance $d\beta$ would lie entirely along the set of $2N - 2$ eigenvectors corresponding to non-zero eigenvalues. In this circumstance, the factor M appearing in Eq. 20 would be replaced by $2N - 2$, generally increasing the magnitude of $\Delta P_{i \rightarrow f}(\beta^*)$. In the present work dimensionless units are used for all variables, thereby avoiding the need for any specific normalization of the Hessian elements. Importantly, the response $\Delta P_{i \rightarrow f}$ is invariant to such a normalization.

2.2.3 Hessian at the Bottom of the Landscape

Although the bottom of the landscape is not a desirable location, behavior there is important to explore as initial controls will likely result in $P_{i \rightarrow f}$ having a small value. Here, we take this to the limit and explore level sets at the absolute bottom corresponding to controls β^* producing $P_{i \rightarrow f} = 0.0$. At the bottom of the landscape, $\langle i|U^\dagger(T, 0)|f \rangle = 0$, utilizing Eqs. 4 and 5 significantly simplifies Eq. 10 to the form

$$\begin{aligned} \frac{\partial^2 P_{i \rightarrow f}}{\partial \beta_j^* \partial \beta_k^*} &= (-2/\hbar^2) \text{Re} \left[\int_0^T \langle q|U^\dagger(t)H_{\beta_j^*}(\beta^*, t)U(t)|i \rangle dt \right. \\ &\quad \left. \times \int_0^T \langle i|U^\dagger(t)H_{\beta_k^*}(\beta^*, t)U(t)|q \rangle dt \right] \end{aligned} \quad (22)$$

where $|q \rangle \equiv U^\dagger(T, 0)|f \rangle$. As for the top of the landscape in Section 2.2.1, once again the Hessian rank at the bottom is important to assess. In order to do so, we define the two vectors $y(\beta^*)$ and $z(\beta^*)$ of length M with entries

$$[y(\beta^*)]_j = \frac{\sqrt{2}}{\hbar} \int_0^T \text{Re}[\langle q|U^\dagger(t, 0)H_{\beta_j^*}(\beta^*, t)U(t, 0)|i \rangle] dt \quad (23a)$$

$$[z(\beta^*)]_j = \frac{\sqrt{2}}{\hbar} \int_0^T \text{Im}[\langle q|U^\dagger(t, 0)H_{\beta_j^*}(\beta^*, t)U(t, 0)|i \rangle] dt. \quad (23b)$$

Then, the Hessian at the bottom may be written explicitly as

$$\nabla^2 P_{i \rightarrow f}(\beta^*) = [y(\beta^*) \cdot y^\top(\beta^*) + z(\beta^*) \cdot z^\top(\beta^*)] \quad (24)$$

and utilizing Eq. 24, the Hessian trace may be expressed as

$$\text{Tr}[\nabla^2 P_{i \rightarrow f}(\beta^*)] = (2/\hbar^2) \sum_{j=1}^M \left| \int_0^T \langle q|U^\dagger(t, 0)H_{\beta_j^*}(\beta^*, t)U(t, 0)|i \rangle dt \right|^2. \quad (25)$$

Similar to the discussion in Section 2.2.1 regarding Eq. 14, now Eq. 24 shows that the rank of the Hessian at the bottom is at most 2. The maximal case of rank 2 occurs if the vectors $y(\beta^*)$ and $z(\beta^*)$ are linearly independent; otherwise, the rank of the Hessian

at the bottom can be less than 2. Thus, at most there are two coordinated variations around the control β^* that will lift $P_{i \rightarrow f}(\beta^*)$ off the bottom, as discussed below.

2.2.4 Climbing Rapidly from the Bottom of the Landscape

At the top of the landscape Section 2.2.2 showed that the Hessian trace is an indicator of the robustness of a control solution. We now similarly show how the Hessian trace may influence gradient climbs originating from controls producing $P_{i \rightarrow f}$ values near the landscape bottom. To exhibit the influence of the Hessian trace on gradient based searches consider a control β' near a control β^* at the bottom of the landscape. Here we assume that β' corresponds to a point slightly off the bottom of the landscape such that $P_{i \rightarrow f}(\beta') > 0.0$. The gradient at $\beta' = \beta^* + d\beta$ can be written as

$$\begin{aligned} \nabla P_{i \rightarrow f}(\beta') &= \nabla P_{i \rightarrow f}(\beta^* + d\beta) \\ &\approx \nabla^2 P_{i \rightarrow f}(\beta^*) \cdot d\beta. \end{aligned} \tag{26}$$

In the present context, $d\beta$ could arise either due to noise or considered as a concerted control variation. The gradient norm squared is

$$\begin{aligned} K(\beta') &\equiv \|\nabla P_{i \rightarrow f}(\beta')\|^2 \\ &\approx \|\nabla^2 P_{i \rightarrow f}(\beta^*) \cdot d\beta\|^2. \end{aligned} \tag{27}$$

At the point β^* at the landscape bottom, the Hessian can be rewritten as

$$\nabla^2 P_{i \rightarrow f}(\beta^*) = \sigma_1 u_1(\beta^*) u_1(\beta^*)^\top + \sigma_2 u_2(\beta^*) u_2(\beta^*)^\top \tag{28}$$

where σ_1 and σ_2 are the two non-zero positive eigenvalues of the Hessian with $u_1(\beta)$ and $u_2(\beta)$ being the corresponding eigenvectors. Then, Eq. 27 becomes

$$K(\beta') = \sigma_1^2 (d\beta^\top \cdot u_1(\beta^*))^2 + \sigma_2^2 (d\beta^\top \cdot u_2(\beta^*))^2. \tag{29}$$

In order to physically interpret Eq. 29 it is convenient to consider a disturbance of unit magnitude $\|d\beta\| = 1$. If $d\beta$ lies entirely in the control space spanned by the two Hessian eigen-directions u_1 and u_2 , then the gradient norm is bounded by σ_1 and σ_2 . However, in the more likely scenario that the vector $d\beta$ also has a component lying in the null space of the Hessian, then the gradient norm is bounded

$$0 \leq \|\nabla P_{i \rightarrow f}(\beta')\| \leq \max\{\sigma_1, \sigma_2\}, \quad \|d\beta\| = 1. \quad (30)$$

Although maximizing the trace of the Hessian does not necessarily imply a larger upper bound for the gradient norm in Eq. 30, experience from numerical simulations (not shown) reveals that strongly curved portions of the landscape bottom generally enable a rapid rise in $P_{i \rightarrow f}$ when aiming at ascent.

3 Algorithms for Landscape Explorations

Previous formal work has shown that level sets of controls exist for all values of $P_{i \rightarrow f}$ including at the top and bottom of the landscape [1, 18, 17]. Each level set member produces the same transition probability value; however, controls over the level set can show a large variation of secondary characteristics. These characteristics may include the mechanism by which control is achieved, the stability of each solution to disturbances, etc. Here, a D-MORPH algorithm is introduced to identify level set members aimed at locating control solutions displaying secondary desirable characteristics in addition to achieving prescribed values of $P_{i \rightarrow f}$. The myopic nature of the D-MORPH algorithm enables the exploration of fundamental landscape issues, as well as provides a link to laboratory landscape excursions. The D-MORPH method has already been implemented in the laboratory where it has been shown to work at the top and bottom of the landscape [19, 20]. We are interested in finding solutions β^* that belong to a level set denoted as \mathcal{L} , corresponding to either $P_{i \rightarrow f}(\beta^*) = 1.0$ or $P_{i \rightarrow f}(\beta^*) = 0.0$.

In order to explore the level set, \mathcal{L} , the control β^* is parametrized with a continuous parameter s , i.e., $\beta^* \Rightarrow \beta^*(s)$. This parameterization can be viewed as a curve $\beta^*(s)$ as a function of s through control space. The initial control $\beta(s = 0)$ is not likely to lie on a level set \mathcal{L} calling for an ascent or descent of the landscape.

The goal of the next section is to derive differential equations for $\beta(s)$ of the form

$$d\beta(s)/ds = F[\beta(s), s]. \quad (31)$$

A particular form of Eq. 31 will produce a trajectory that can ascend/descend to the landscape top/bottom starting from an initial control β while another form of Eq. 31 will produce a *trajectory* $\beta^*(s) \in \mathcal{L}$ that lies on the level set maintaining either $P_{i \rightarrow f}(\beta^*(s)) = 1.0$ or $P_{i \rightarrow f}(\beta^*(s)) = 0.0$ upon starting from an initial point at the respective landscape extremum. Section 3.1 presents the differential equation for ascending or descending the landscape and Section 3.2 presents the algorithm for exploring the level sets at values of $P_{i \rightarrow f} = 1.0$ and $P_{i \rightarrow f} = 0.0$. Section 3.3 shows that the D-MORPH algorithm may be utilized to locate solutions exhibiting secondary desirable physical characteristics along level sets at either $P_{i \rightarrow f} = 1.0$ or 0.0 .

3.1 Ascending and Descending the Landscape

Exploring level sets at the top or bottom of the landscape first necessitates finding an initial control residing at either location. For this purpose, the D-MORPH technique can be used to ascend or descend the landscape from an arbitrary trial control $\beta(0)$. Differentiating $P_{i \rightarrow f}(s) = P_{i \rightarrow f}(\beta(s))$ with respect to s produces

$$dP_{i \rightarrow f}(\beta(s))/ds = \nabla P_{i \rightarrow f}(\beta(s))^T \cdot d\beta(s)/ds. \quad (32)$$

Choosing

$$\partial\beta(s)/\partial s = \rho(s)\nabla P_{i \rightarrow f}(\beta(s)) \quad (33)$$

for $\rho(s) > 0$ guarantees ascension since $dP_{i \rightarrow f}(s)/ds \geq 0$; while choosing $\rho(s) < 0$ will result in descension. The function $\rho(s)$ may be chosen as desired, and its magnitude will dictate the rate of ascent or descent. Equation 32 will be used to identify controls β^* residing at the landscape top and bottom.

3.2 Movement on the Top and Bottom Level Sets

This section is concerned with movement along the level set of control solutions either at the bottom or top of the control landscape, corresponding to $\beta^*(s)$ values maintaining either $P_{i \rightarrow f}(\beta^*(s)) = 0.0$ or $P_{i \rightarrow f}(\beta^*(s)) = 1.0$. In order to derive an equation for the desired trajectories, we take into account that the first derivative $\nabla P_{i \rightarrow f}(\beta^*)$ is necessarily zero at the top or bottom of the landscape and therefore differentiate $P_{i \rightarrow f}(\beta^*(s))$ twice with respect to s ,

$$d^2 P_{i \rightarrow f}(\beta^*(s))/ds^2 = (1/2) (\partial \beta^*(s)/\partial s)^\top \cdot \nabla^2 P_{i \rightarrow f}(\beta^*(s)) \cdot (\partial \beta^*(s)/\partial s). \quad (34)$$

Investigating the trajectories $\beta^*(s)$ over the top or bottom of the landscape is assured by demanding that $d^2 P_{i \rightarrow f}(\beta^*(s))/ds^2 = 0$.

The analysis in Sections 2.2.1 and 2.2.3, showed that the rank of the Hessian is at most $L = 2N - 2$ and $L = 2$ at the top and bottom, respectively. Since the Hessian $\nabla^2 P_{i \rightarrow f}$ is a real symmetric $M \times M$ matrix, it has M real eigenvalues. The Hessian rank being L , with generally $L < M$, means that there are additionally $M - L$ zero eigenvalues. Thus, the Hessian can be written as

$$\nabla^2 P_{i \rightarrow f}(\beta^*(s)) = \sum_{\ell=1}^L \sigma_\ell u_\ell(\beta^*(s)) \cdot u_\ell^\top(\beta^*(s)). \quad (35)$$

where the $\{u_\ell(\beta^*(s))\}$ are the orthonormal eigenvectors of $\nabla^2 P_{i \rightarrow f}(\beta^*(s))$ corresponding to the L non-zero eigenvalues, σ_ℓ .

Using Eqs. 34 and 35, the criterion $d^2 P_{i \rightarrow f}(s)/ds^2 = 0$ specifies the following L

linear constraints on $d\beta^*(s)/ds$

$$u_\ell(\beta^*(s))^\top \cdot d\beta^*(s)/ds = 0 \quad \ell = 1, \dots, L. \quad (36)$$

The constraints given by Eq. 36 can be re-expressed as a differential equation whose solution is a trajectory $\beta^*(s)$ on the level set \mathcal{L} at either the top or bottom of the landscape,

$$d\beta^*(s)/ds = \hat{P}^c(\beta^*(s)) \cdot g(\beta^*(s), s), \quad (37)$$

where $g(\beta^*(s), s)$ is a vector of length M that can be freely chosen. The projector \hat{P}^c is specified by its action

$$\hat{P}^c(\beta^*(s)) \cdot g(\beta^*(s), s) \equiv g(\beta^*(s), s) - \sum_{\ell} u_\ell(\beta^*(s)) [u_\ell(\beta^*(s))^\top \cdot g(\beta^*(s), s)] \quad (38)$$

which removes any component of the vector $g(\beta^*(s), s)$ lying in the space spanned by the set of eigenvectors $\{u_\ell(\beta^*(s))\}$. Thus, $\hat{P}^c(\beta^*(s))$ is the projector onto the null space of $\nabla^2 P_{i \rightarrow f}(\beta^*(s))$ thereby assuring that the solution of Eq. 37, $\beta^*(s)$, will satisfy the constraints in Eq. 36; direct substitution of Eq. 37 into Eq. 36 upon use of Eq. 38 shows that the demand $u_\ell(\beta^*(s))^\top \cdot d\beta^*(s)/ds = 0$ is satisfied. The choice of free vector $g(\beta^*(s), s)$ will specify the particular trajectory on the level set.

3.3 Particular Control Trajectories at the Top or Bottom of the Landscape to Meet Auxiliary Objectives

The freedom in choosing the vector g in Eq. 37 will lead to different D-MORPH trajectories over the top or bottom level sets. This freedom allows for secondary control behavior demands to be placed on level set explorations. For example, solutions may be sought that achieve high yield while either minimizing the effects of parameter disturbances on the overall outcome, minimizing the pulse fluence or optimizing other

physical properties.

Consider, for example, the goal of moving on the level set \mathcal{L} while also seeking to maximize a secondary cost function $J(\beta^*)$, such as robustness to variations $\beta^* \rightarrow \beta^* + d\beta$ at the top of the landscape. As the trajectory specified by the solution to Eq. 37 advances, changes in J will be given by

$$dJ(s)/ds = \nabla J(\beta^*(s))^\top \cdot d\beta^*(s)/ds, \quad (39)$$

and substituting Eq. 37 into Eq. 39 gives

$$dJ(s)/ds = \nabla J(\beta^*(s))^\top \cdot \hat{P}^c(\beta^*(s)) \cdot g(\beta^*(s), s). \quad (40)$$

As the projector $\hat{P}^c(\beta^*(s))$ is positive semi-definite, choosing $g(\beta^*(s), s) = \rho'(s)\nabla J(\beta^*(s))$, with $\rho'(s) > 0$ will locally maximize J over the trajectory constrained to the level set \mathcal{L} and the value of $\rho'(s)$ will mediate the rate that J rises in the process. Similarly, choosing $\rho'(s) < 0$ will lead to minimization of J over the level set \mathcal{L} .

4 Illustrations

Exploring the level sets at the top or bottom necessitates first either ascending or descending the landscape with Eq. 33. Upon reaching either $P_{i \rightarrow f} = 1.0$ or $P_{i \rightarrow f} = 0.0$ (within adequate tolerance), we then move over the associated level set by solving the second-order D-MORPH equation in Eq. 37. The D-MORPH ascent/descent Eq. 33 is solved using a Runge-Kutta fourth-order variable step size integrator over the s -domain. The second-order D-MORPH Eq. 37 is solved using the same integrator until $P_{i \rightarrow f}$ deviates beyond a specified tolerance, δ , from the level set value. In the following examples, the *top* of the landscape is defined as $P_{i \rightarrow f} > 1 - \delta$ and the *bottom* of the landscape as $P_{i \rightarrow f} < \delta$ where $\delta = 10^{-8}$. If the tolerance is violated, a switch to the first order ascent/descent Eq. 33 is made to, respectively, ascend or descend back to

the level set at the top or bottom.

The examples explore the top and bottom of the landscape for Hamiltonians of the form

$$H(t) = H_0 - \mu\epsilon(t). \quad (41)$$

where H_0 is diagonal, μ is a real symmetric dipole matrix and $\epsilon(t)$ is the electric control field,

$$\epsilon(t) = S(t) \sum_{ij}^P a_{ij} \sin(\omega_{ij}t + \phi_{ij}) \quad (42)$$

with P contributing frequencies and the envelope

$$S(t) = \exp \left\{ -\frac{(t - T/2)^2}{2\sigma^2} \right\}. \quad (43)$$

The indices ' ij ' in Eq. 42 correspond to the system transition frequencies and are explicitly stated for each particular illustration below. We set $\sigma = 3.5$ in the simulations. The control variables β are drawn from (a) the set of Hamiltonian structure parameters $\{E_j, \mu_j, \mu_{ij}\}$ where E_j is the j -th system energy level and μ_j and μ_{ij} are diagonal and off-diagonal dipole matrix elements, respectively, and (b) the field parameters $\{a_{ij}, \phi_{ij}\}$ where a_{ij} is the amplitude and ϕ_{ij} the phase associated with the ω_{ij} spectral component. The goal is to explore controls at the top or bottom of the landscape through the Hamiltonian structure variables of H_0 and μ in Eq. 41, and/or the applied field through the amplitudes and phases in Eq. 42. In these simulations, dimensionless units are used, \hbar is set to 1.0, and time is discretized between $t = 0$ and $T = 20$ into 4096 points. The selected cases below are chosen to illustrate basic physical behavior at the top and bottom of the landscape that was identified in an extensive set of simulations.

4.1 Level Sets at the Top of the Hamiltonian Structure Control Landscape

Here, we consider a simple $N = 2$ state system with $M = 3$ Hamiltonian structure control variables E_2, μ_2 and μ_{12} along with a fixed electric field $\epsilon(t)$. This simple system is chosen for investigation as it permits a clear picture of level set exploration at the top of the landscape.

For illustration, seven distinct initial systems specified by the values of E_2, μ_2 and μ_{12} were generated with each being a point on the top of the landscape. The fixed field, $\epsilon(t)$ was chosen using the form in Eq. 42 with $P = 4$, and $\epsilon(t)$ merely serves the role of facilitating utilization of the controls E_2, μ_2 and μ_{12} . The field parameters are given in [21]. As initial systems, we chose $E_2 = \mu_2 = 0$ and a simple search over μ_{12} was performed to find that $\mu_{12} = \{0.14, 0.42, 0.70, 0.98, 1.26, 1.54, 1.82\}$ satisfy $P_{i \rightarrow f} = 1.0$ [11]. Following the discussion in Section 2.2.1, the rank of the Hessian at the top of the landscape was confirmed numerically to be $2N - 2 = 2$. Thus, with three controls, there is an underlying one dimensional level set satisfying $P_{1 \rightarrow 2} = 1.0$; the level set is a curve $\{E_2(s), \mu_2(s), \mu_{12}(s)\}$ parameterized by s lying in the three dimensional control space.

In the simulations, the free vector $g(\beta^*(s), s)$ in Eq. 37 was chosen to be the eigenvector $u^0(\beta^*(s))$ corresponding to the only non-zero eigenvalue of the Hessian. Since the eigenvectors of the Hessian are orthogonal, this choice of free vector corresponds to simply moving in the direction given by $u^0(\beta^*(s))$. The integration of Eq. 37 was performed over the domain $s \in [0, 20]$. Starting from the initial points $\{E_2(0), \mu_2(0), \mu_{12}(0)\}$ above, Fig. 2 shows the seven one dimensional trajectories with each tracing out a path on the level set at the top of the landscape, $P_{1 \rightarrow 2} = 1.0$. Each level set trajectory is seen to be a highly coordinated path through the space of controls E_2, μ_2 and μ_{12} . Although it is possible that the seven paths actually are segments of a single overall level set trajectory (i.e., the paths eventually join together)

this circumstance was not found to be the case over the domain explored here. Thus, Fig. 2 also illustrates that level sets *may* have disconnected components. The highly contorted nature of the level set trajectories in Fig. 2 illustrates the complex structure of the top of the landscape.

4.2 Robustness at the Top of the Combined Hamiltonian Structure and Field Control Landscape

In this section, we explore the robustness of an $N = 5$ level system with fixed diagonal H_0 energies $E_1 = 0, E_2 = 1, E_3 = 4, E_4 = 9, E_5 = 16$. There are $M = 12$ total controls β^* drawn from: the dipole matrix elements, $\{\mu_{j,j+1}\}_{j=1,\dots,4}$ as well as the field amplitudes $\{a_{j,j+1}\}_{j=1,\dots,4}$ and phases $\{\phi_{j,j+1}\}_{j=1,\dots,4}$. The remaining dipole elements and field amplitudes and phases were fixed at zero. The frequency associated with the $j \rightarrow j + 1$ transition is given by $\omega_{j,j+1} = |E_{j+1} - E_j|$ and the field had the form in Eq. 42 with $P = 4$.

In this illustration, the trajectory of controls $\beta^*(s)$ was determined with an extra cost as the trace of the Hessian,

$$J = \text{Tr}(\nabla^2 P_{i \rightarrow f}) = \sum_{j=1}^{12} \frac{\partial^2 P_{i \rightarrow f}}{\partial \beta_j^{*2}} = \sum_{\ell=1}^8 \sigma_\ell < 0, \quad (44)$$

introduced to explore the curvature of the level set at the top of the landscape, $P_{1 \rightarrow 5} = 1.0$. The value of J directly influences the robustness to variations in the controls $d\beta$ as evident from J being the sum of the Hessian eigenvalues, σ_ℓ . An initial control at the top of the landscape was found through Eq. 33 with $\rho(s) = 1.0$ starting from the initial set of four amplitudes, phases and dipoles given in [22]. The ascent procedure converged to the nominal control value β_0^* denoting the amplitudes, phases and dipole values producing $P_{1 \rightarrow 5} \simeq 1.0$. In the ascent J was not explicitly considered, but its value of $J = -180.9$ was recorded at β_0^* as a reference for comparison. The nominal

control variables, β_0^* , were used as the initial condition for a calculation designed to locate the most robust solution, β_{rob}^* at the top of the landscape. Following the logic in Section 3.3, the free vector in Eq. 37 was chosen as $g_{\text{rob}}(\beta^*(s)) = \nabla J(\beta^*(s))$, i.e., β_{rob}^* corresponds to the smallest attained value of $|J|$, as $J < 0$. This choice of free vector follows from the discussion of robustness in Section 2.2.2. The gradient $\nabla J(\beta^*(s))$ was calculated using a finite difference scheme. The solution β_0^* , producing $J = -180.9$ along with the solution β_{rob}^* producing $J = -30.3$ are shown in Fig. 3a and 3b., respectively.

To investigate the robustness of the control β^* at the landscape top, the Hessian matrix for the solutions β_0^* and β_{rob}^* was calculated with Eq. 14. The Hessian eigenvalue of largest magnitude was -69.7 for β_0^* while the corresponding value was -14.1 for β_{rob}^* . The eigenvector associated with the largest magnitude eigenvalue for both solutions is plotted in Fig 4. Fig. 4a shows that the control solution β_0^* is most sensitive to decreasing the magnitude of the dipoles μ_{12} and μ_{23} . In contrast, Fig. 4b shows that the control solution β_{rob}^* is most sensitive to decreasing the magnitude of the amplitude a_{45} and the dipole μ_{45} (the nominal value of $\mu_{45} < 0$ in Fig. 3b) as well as increasing the magnitude of a_{34} and μ_{34} .

Together, Figs. 3 and 4 show the manner in which a more robust solution was established. Over the level set trajectory (i.e., on going from Fig. 3a to Fig. 3b), the magnitude of the field amplitudes were decreased by $\sim 70\%$ while the magnitude of the dipoles were increased by approximately the same amount. This *redistribution* of parameter magnitude produces a more stable solution at the top of the landscape. The small magnitude of the dipole matrix elements in Fig 3a lead to very unstable solutions when amplitude, phase and dipole matrix element noise is introduced into the system. This is evident from the large eigenvector contribution of μ_{12} and μ_{23} in Fig. 4a. Conversely, the balanced distribution of about equal magnitude for the field amplitudes and dipole elements in Fig 3b provides a more stable solution. Although the changes in the phases are more subtle to interpret, the optimization process manipulated these

as well in order to gain robustness.

In order to assess the degree of robustness of the control solutions, a simulation was run to test the effect of random disturbances around β_0^* and β_{rob}^* . Disturbances were introduced by selecting a random vector, p_{rand} , where each entry was chosen from a normal distribution with zero mean and standard deviation of 1.0. Then p_{rand} was normalized to produce $\|p_{\text{rand}}\| = 0.25$. For 5000 runs, the control solutions β_0^* and β_{rob}^* were perturbed by the same random vector, e.g., $\beta' = \beta^* + p_{\text{rand}}$, and $P_{1 \rightarrow 5}(\beta')$ was recorded. The results are given in Fig. 5 where panel (a) corresponds to β_0^* and panel (b) corresponds to β_{rob}^* .

Figure 5 shows that the nominal control solution in panel (a) is highly sensitive to the perturbations introduced by p_{rand} while the robust control solution in panel (b) is minimally sensitive to the random perturbations introduced by p_{rand} . Although both control solutions are able to achieve a very high yield, $P_{1 \rightarrow 5} \simeq 1.0$, only the solution in panel (b) can tolerate significant disturbances in the parameter settings. The mean value of $P_{1 \rightarrow 5}$ for panel (a) is 0.612 with a left standard deviation of 0.174 while the mean value of $P_{1 \rightarrow 5}$ for panel (b) is 0.936 with a left standard deviation of 0.040. Additional tests of robustness were performed on these control solutions including stability to relative disturbances, i.e., $\beta' = \beta^*(1 + p_{\text{rand}})$ that confirmed the robustness of β_{rob}^* over that of β_0^* (not shown) but to a lesser degree.

4.3 The Ease of Climbing off the Bottom of the Control Field Landscape

The bottom of the landscape is a domain where the goal is to ascend as rapidly as possible. As $\nabla P_{i \rightarrow f} = 0$ at the bottom, the curvature dictates the rate of climbing. Thus, in this example, we investigate the curvature extremes encountered at the landscape bottom for the target $1 \rightarrow 3$ transition by analyzing the trace of the Hessian over families of control solutions producing $P_{1 \rightarrow 3} = 0.0$. An $N = 4$ state system is consid-

ered with fixed H_0 and μ specified by $E_1 = 0.0, E_2 = 1.0, E_3 = 4.0, E_4 = 9.0, \mu_{12} = 0.50, \mu_{13} = 0.25, \mu_{14} = 0.15, \mu_{23} = 0.20, \mu_{24} = 0.10, \mu_{34} = 0.05$, and the control field for variation has the form in Eq. 42 with $P = 6$ corresponding to $M = 12$ amplitude and phase control variables. An initial control solution, β_0^* , was found producing $P_{1 \rightarrow 3} = 0.0$ using the descent procedure in Eq. 33 with $\rho(s) = -1.0$, and two separate D-MORPH runs were initiated at β_0^* with the goals of either maximizing or minimizing the Hessian trace, $J = \text{Tr}[\nabla^2 P_{i \rightarrow f}]$, in Eq. 25 while remaining at the bottom of the landscape. Here, the free vector in Eq. 37 is chosen as $g = \pm \nabla J$, with $+$ for maximization and $-$ for minimization of the Hessian trace. The control field solution that maximized the Hessian trace produced β_{\max}^* with $J = 8 \times 10^3$, while the solution that minimized the Hessian trace produced β_{\min}^* with $J = 0.31$.

Figure 6 shows the dynamics of state $|3\rangle$ induced by both control solutions where the value $P_{1 \rightarrow 3} \simeq 0.0$ is reached at the final time. Contrary to what might be expected, the population of state $|3\rangle$ over time is non-trivial at the landscape bottom with dynamics varying greatly over the breadth of the level set. In particular, $P_{1 \rightarrow 3}(t)$ for the maximal trace control solution, β_{\max}^* , significantly lifts off the bottom at intermediate times to only finally return to $P_{1 \rightarrow 3} \simeq 0.0$ at the final target time. In contrast, the minimal trace control solution, β_{\min}^* , has $P_{1 \rightarrow 3}(t) \simeq 0.0$ over the full time interval $0 \leq t \leq 20$. Moreover, from these simulations, the mean Hessian eigenvalue at the most curved portion of the level set, corresponding to β_{\max}^* , is found to be more than three orders of magnitude larger than the mean eigenvalue at the flattest portion of the level set corresponding to β_{\min}^* .

To investigate the influence of the curvature at the landscape bottom on attempts to climb from there ($P_{i \rightarrow f} \approx 10^{-8}$), two gradient ascents were initiated, respectively, originating from the maximal and minimal trace producing fields. These were done over the interval $s \in [0, 2]$ using Eq. 33 with $\rho(s) = 1$ and the results are shown in Fig. 7. The gradient ascent starting at the maximal trace field β_{\max}^* (corresponding to the left-ordinate) reaches a maximum value of $P_{1 \rightarrow 3} \approx 0.999$ at the final time and

$s = 2$ while the gradient ascent starting at the minimal trace field β_{\min}^* (corresponding to the right-ordinate) reaches a maximum value of $P_{1 \rightarrow 3} \approx 9.5 \times 10^{-9}$ at the final time and $s = 2$. Here, and in a large number of other simulations, it is evident that the trace of the Hessian at the bottom of the control landscape has a significant influence on the rapidity with which searches can ascend from there. On the abscissa scale in Fig. 7, the optimization starting from the minimal trace field β_{\min}^* reaches a value of $P_{1 \rightarrow 3} > 0.9$ only at $s \approx 68$.

These results on the varying degrees of curvature at the landscape bottom are significant because most searches for effective control fields start out with low yields. This circumstance is especially important for complex systems where no intuitive set of good trial controls may exist to begin the optimization procedure. However, these simulations also show that there can be attractive classes of trial controls corresponding to extremely curved portions of the control landscape at the bottom.

5 Conclusion

This work considered the transition probability landscape as a function of either the Hamiltonian structure and/or an applied field. Level sets were shown to exist at the landscape top $P_{i \rightarrow f} = 1.0$ and bottom $P_{i \rightarrow f} = 0.0$. Each level set can contain control solutions displaying a range of secondary characteristics, including robustness to disturbances at the top and rapid climbing capability from the bottom. We also introduced an extended version of the D-MORPH algorithm for identifying desirable control solutions at the landscape top or bottom. This advance complements the prior algorithm [9] for exploring transition probability values over the interior domain $0 < P_{i \rightarrow f} < 1.0$. Taken together, these D-MORPH algorithms provide the means to explore the control landscape and its level sets at any value of $P_{i \rightarrow f}$ to gain fundamental insights as well as for the practical concerns of finding robust control solutions.

Although the D-MORPH procedure was developed here in a theoretical and compu-

tational context, it is also possible to extend some of the core concepts to the laboratory where statistical sampling of the controls [19] can be used to obtain first (gradient) and second-order (Hessian) information (i.e., either by varying the applied field or Hamiltonian structure). In particular, this procedure has been used to measure the Hessian at the top and bottom of the $N = 4$ level atomic Rubidium landscape and travel along the associated level sets [20]. A general procedure might implement a closed-loop technique coupled to a learning algorithm capable of *updating* the field and Hamiltonian parameters progressively towards an optimal set at the top or bottom [23] especially for more complex systems.

The ability to explore ancillary goals (e.g., robustness to field noise or Hamiltonian structure variations illustrated here) at the highest (and lowest) yields reveals additional glimpses of the fundamental control landscape. Other ancillary goals can be envisioned including those that place demands on the nature of the mechanism that achieves the control goal. For example, if the target is controlled rearrangement of a molecule then a cost can be placed against populating any states that lead to dissociation or other undesirable physical processes. Although this study focused on the transition probability landscape, the concepts here can be applied to the quantum control landscape for any observable. Furthermore, these tools can be extended to address an ensemble of systems using the density matrix formalism.

Acknowledgements

The authors acknowledge funding from the DOE and ARO. J.D. acknowledges funding from the Program in Plasma Science and Technology.

References

- [1] H. A. Rabitz, M. M. Hsieh, and C. M. Rosenthal, “Quantum Optimally Controlled Transition Landscapes,” *Science*, vol. 303, no. 5666, pp. 1998–2001, 2004.
- [2] A. Assion, T. Baumert, M. Bergt, T. Brixner, B. Kiefer, V. Seyfried, M. Strehle, and G. Gerber, “Control of Chemical Reactions by Feedback-Optimized Phase-Shaped Femtosecond Laser Pulses,” *Science*, vol. 282, no. 5390, pp. 919–922, 1998.
- [3] M. Roth, L. Guyon, J. Roslund, V. Boutou, F. Courvoisier, J.-P. Wolf, and H. Rabitz, “Quantum control of tightly competitive product channels,” *Physical Review Letters*, vol. 102, no. 25, p. 253001, 2009.
- [4] J. Kunde, B. Baumann, S. Arlt, F. Morier-Genoud, U. Siegner, and U. Keller, “Adaptive feedback control of ultrafast semiconductor nonlinearities,” *Applied Physics Letters*, vol. 77, no. 7, pp. 924–926, 2000.
- [5] J. Herek, “Coherent control of photochemical and photobiological processes,” *Journal of Photochemistry and Photobiology A-Chemistry*, vol. 180, no. 3, 2006.
- [6] T. Weinacht and P. Bucksbaum, “Controlling the Shape of a Quantum Wavefunction,” *Nature*, vol. 397, no. 233, 1999.
- [7] K. Moore, M. Hsieh, and H. Rabitz, “On the relationship between quantum control landscape structure and optimization complexity,” *The Journal of Chemical Physics*, vol. 128, no. 15, p. 154117, 2008.
- [8] Z. Shen, M. Hsieh, and H. Rabitz, “Quantum optimal control: Hessian analysis of the control landscape,” *The Journal of Chemical Physics*, vol. 124, no. 20, p. 204106, 2006.
- [9] A. Rothman, T.-S. Ho, and H. Rabitz, “Quantum observable homotopy tracking control,” *The Journal of Chemical Physics*, vol. 123, no. 13, p. 134104, 2005.

- [10] A. Rothman, T.-S. Ho, and H. Rabitz, “Exploring the level sets of quantum control landscapes,” *Physical Review A (Atomic, Molecular, and Optical Physics)*, vol. 73, no. 5, p. 053401, 2006.
- [11] A. Donovan, V. Beltrani, and H. Rabitz, “Quantum control by means of hamiltonian structure manipulation,” *Phys. Chem. Chem. Phys.*, 2011. DOI: 10.1039/c0cp02234a.
- [12] V. Jurdjevic and H. J. Sussmann, “Control systems on lie groups,” *Journal of Differential Equations*, vol. 12, no. 2, pp. 313 – 329, 1972.
- [13] V. Ramakrishna, M. V. Salapaka, M. Dahleh, H. Rabitz, and A. Peirce, “Controllability of molecular systems,” *Phys. Rev. A*, vol. 51, pp. 960–966, Feb 1995.
- [14] F. Albertini and D. D’Alessandro, “Notions of controllability for quantum mechanical systems,” in *Decision and Control, 2001. Proceedings of the 40th IEEE Conference on*, vol. 2, pp. 1589–1594 vol.2, 2001.
- [15] A. Rothman, T.-S. Ho, and H. Rabitz, “Observable-preserving control of quantum dynamics over a family of related systems,” *Physical Review A (Atomic, Molecular, and Optical Physics)*, vol. 72, no. 2, p. 023416, 2005.
- [16] J.-T. Hwang and H. Rabitz, “The green’s function method of sensitivity analysis in quantum dynamics,” *The Journal of Chemical Physics*, vol. 70, no. 10, pp. 4609–4621, 1979.
- [17] T.-S. Ho and H. Rabitz, “Why do effective quantum controls appear easy to find?,” *Journal of Photochemistry and Photobiology A: Chemistry*, vol. 180, no. 3, p. 226, 2006.
- [18] H. Rabitz, T.-S. Ho, M. Hsieh, R. Kosut, and M. Demiralp, “Topology of optimally controlled quantum mechanical transition probability landscapes,” *Physical Review A (Atomic, Molecular, and Optical Physics)*, vol. 74, no. 1, p. 012721, 2006.

- [19] J. Roslund and H. Rabitz, “Gradient algorithm applied to laboratory quantum control,” *Physical Review A (Atomic, Molecular, and Optical Physics)*, vol. 79, no. 5, p. 053417, 2009.
- [20] J. Roslund, *Quantum Control in the Laboratory*. Princeton University, 2010.
- [21] Since the system energies are permitted to vary, there is no natural labeling of frequencies. Here, we just list the frequencies chosen, along with the corresponding amplitudes and phases. Frequencies = $\{1.10, 0.16, 0.07, 1.00\}$. Amplitudes = $\{1.61, 2.25, 0.74, 2.07\}$. Phases = $\{-1.15, -0.11, -1.71, -0.46\}$.
- [22] The initial set of amplitudes, phases and dipoles produced $P_{i \rightarrow f} \approx 0.0$ and were given by: $a_{12} = 1.80, a_{23} = 2.94, a_{34} = 1.33, a_{45} = 1.38, \phi_{12} = 1.65, \phi_{23} = 0.88, \phi_{34} = 2.95, \phi_{45} = 3.09, \mu_{12} = -1.00, \mu_{23} = -0.72, \mu_{34} = -0.35, \mu_{45} = 0.05$.
- [23] R. S. Judson and H. Rabitz, “Teaching lasers to control molecules,” *Phys. Rev. Lett.*, vol. 68, pp. 1500–1503, Mar 1992.

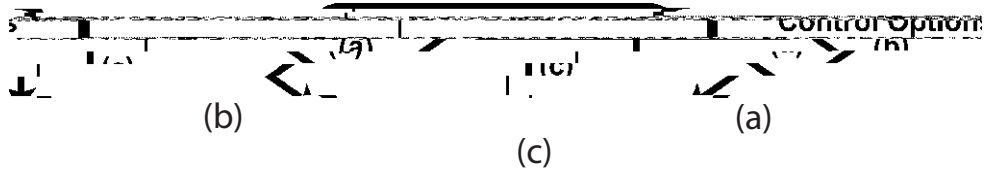


Figure 1

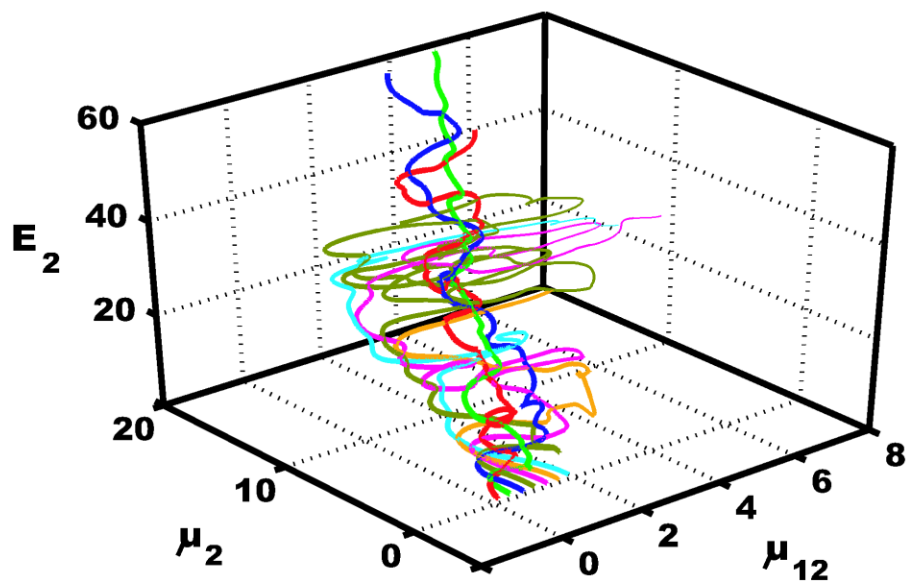


Figure 2

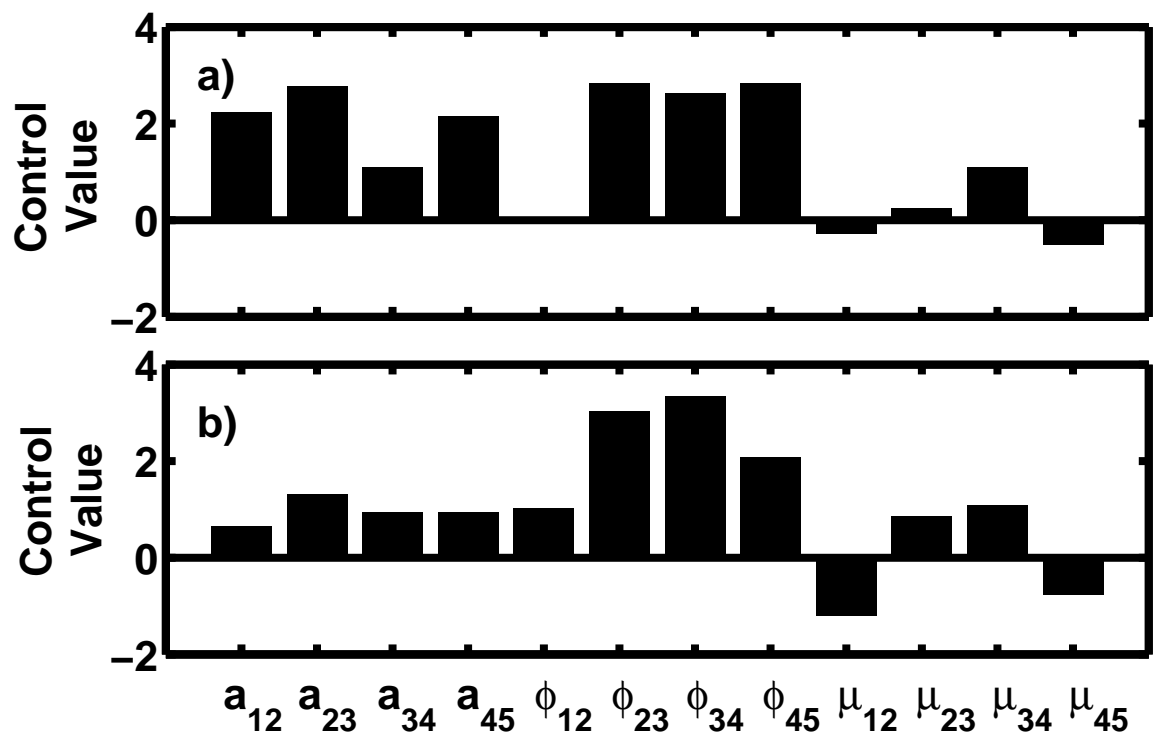


Figure 3

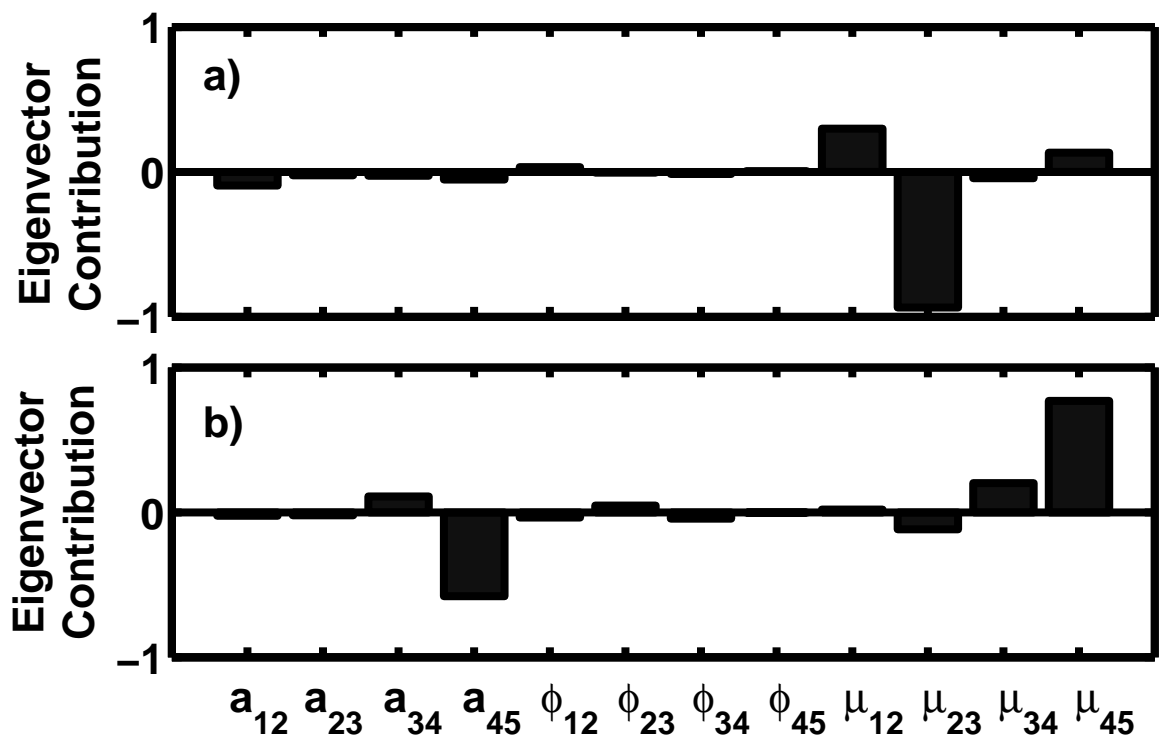


Figure 4

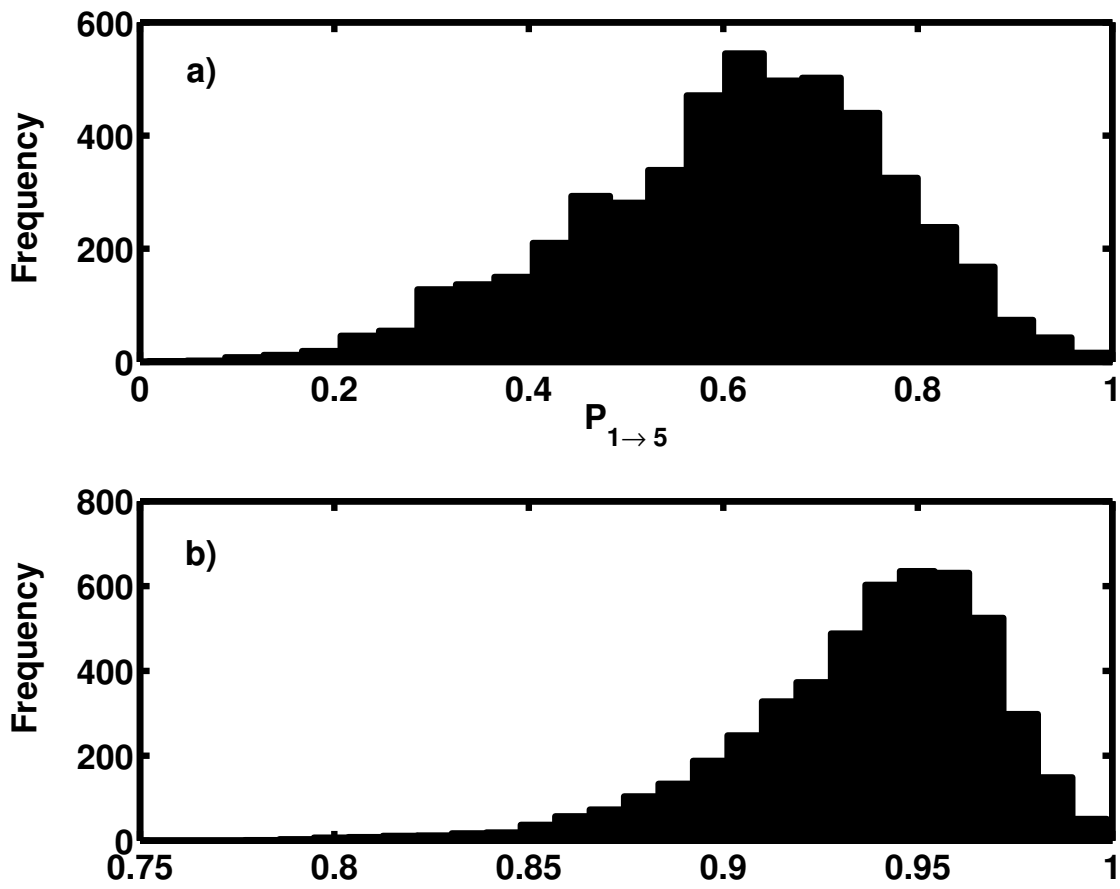


Figure 5

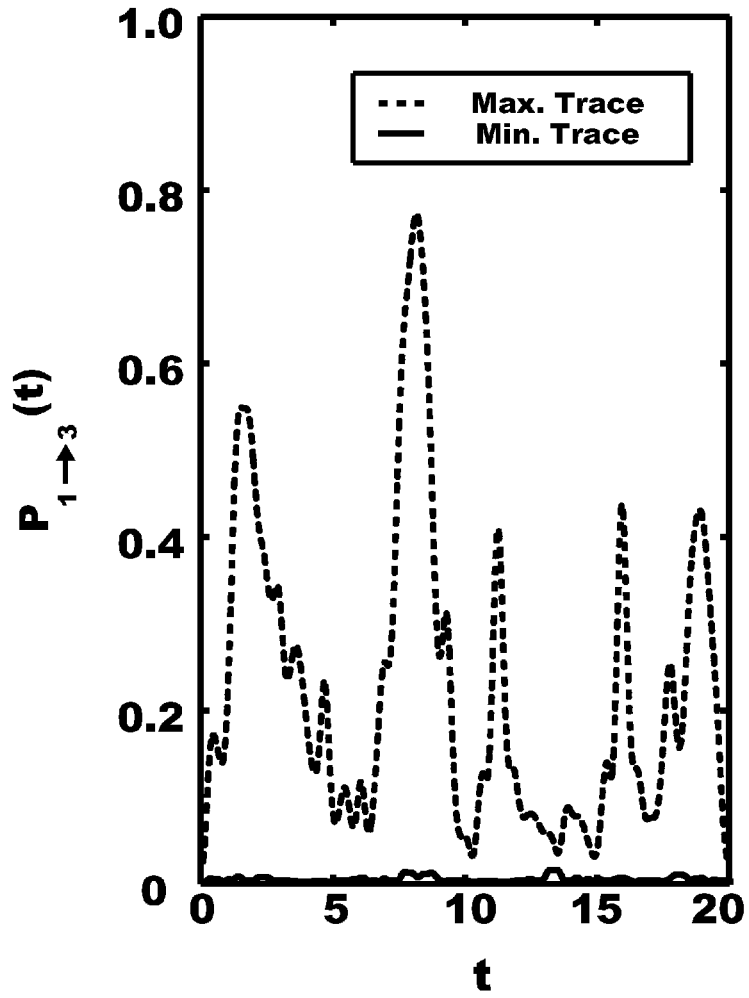


Figure 6

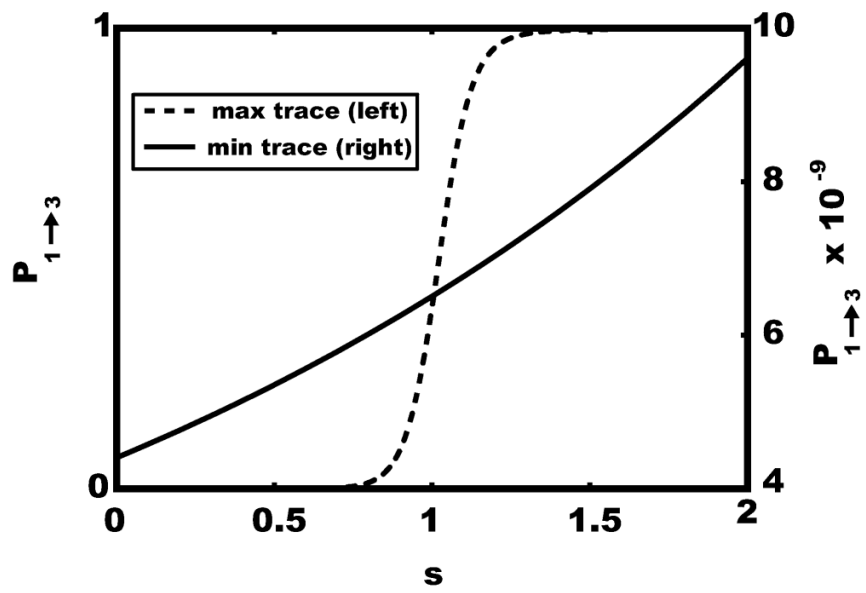


Figure 7

Figure 1

Diagram of control variable options drawn from the Hamiltonian. (a) The traditional view of quantum control where the applied field is the control and the Hamiltonian structure is fixed. (b) The control is the Hamiltonian structure (e.g., energy level spacings and couplings) and the corresponding dynamics are facilitated by a fixed applied control field. In this case, the landscape is explored by traversing the Hamiltonian structure controls. (c) Both the Hamiltonian structure and the applied field are the controls. The overall purview in (c) reveals the richness in considering controls through access to molecular/material samples and external fields. With a suitable choice of controls, the entire observable landscape is subject to exploration, including the level sets at the top and bottom.

Figure 2

The $P_{1 \rightarrow 2} = 1$ level set at the top of the Hamiltonian structure landscape for an $N = 2$ state system in Section 4.1 with controls given by E_2, μ_2 and μ_{12} . A fixed applied field $\epsilon(t)$ is present facilitating the dynamics of the system. Every point along each trajectory corresponds to a control set E_2, μ_2, μ_{12} that accomplishes perfect yield under the influence of the same field. Each of the seven level set curves start with $E_2 = 0, \mu_2 = 0$ and a particular point along the μ_{12} axis.

Figure 3

Values of the control variables for the nominal β_0^* and robust β_{rob}^* control solutions for the example in Section 4.2 at the top of the landscape for $P_{1 \rightarrow 5} = 1.0$. These parameter settings correspond to field amplitudes and phases, as well as the dipole couplings as discussed in the text. The control β_0^* in (a) produces a Hessian trace of -180.9 , while the control β_{rob}^* in (b) produces a Hessian trace of -30.3 .

Figure 4

Largest eigenvector of the Hessian at the top of the landscape ($P_{1 \rightarrow 5} = 1$) for the nominal and robust control solutions (a) β_0^* and (b) β_{rob}^* , respectively, from the example in Section 4.2 and Fig. 3. In (a) the eigenvector for the nominal case has a corresponding eigenvalue of -69.7 while in (b) the eigenvector for the most robust case has a corresponding eigenvalue of -14.1 . The nominal control solution shows sensitivity to nearly every dipole value. The robust control solution shows a significant sensitivity to the amplitudes a_{34} and a_{45} , as well as the corresponding dipole elements.

Figure 5

Distribution of $P_{1 \rightarrow 5}$ values after perturbing (a) the nominal control solution β_0^* and (b) the robust control solution β_{rob}^* with Gaussian distributed variations of each control variable for the example discussed in Section 4.2 and Fig. 4. The mean $P_{1 \rightarrow 5}$ value for (a) is 0.612 with left standard deviation 0.174 . Note the distinct abscissa scales in (a) and (b). The mean $P_{1 \rightarrow 5}$ value for (b) is 0.936 with left standard deviation 0.040 .

Figure 6

Population of state $|3\rangle$ over time, $P_{1 \rightarrow 3}(t)$, for the control field producing either a Hessian maximal or minimal trace at the bottom of the landscape for the example in Section 4.3. The minimal trace field induces dynamics that keep the population in state $|3\rangle$ from ever exceeding 0.03 while the maximal trace field produces much more complex dynamics with large population spikes over the time interval. Both control fields result in a final value, $P_{1 \rightarrow 3} \approx 4 \times 10^{-9}$ on the level set bottom at the final time.

Figure 7

Results of two separate gradient ascents of the control landscape using Eq. 33 over the fixed range $s \in [0, 2]$ starting near the bottom ($P_{i \rightarrow f} < 10^{-8}$) of the applied field landscape for the example in Section 4.3 and Fig. 6. The ascents start at different

locations on the landscape bottom corresponding to fields producing a Hessian trace of either maximal value (dashed: left-axis) or minimal value (solid: right-axis). Both initial control fields produce $P_{1 \rightarrow 3} < 10^{-8}$ at $s = 0$ and, in both cases, the goal is to rapidly increase $P_{1 \rightarrow 3}$. At $s = 2$, the ascent originating from the maximal trace field (trace = 8×10^3) reaches a value of $P_{1 \rightarrow 3} \approx 0.999$, whereas the ascent originating from the minimal trace field (trace = 0.31) just reaches a value of $P_{1 \rightarrow 3} \approx 9.5 \times 10^{-9}$. On the scale of the abscissa, the ascent for the minimal trace field reaches $P_{1 \rightarrow 3} > 0.9$ only at $s \approx 68$.